Quadrobee: Simulating Flapping Wing Aerial Vehicle Dynamics On A Quadrotor

Yuyang Chen[1], Sawyer B. Fuller[2] and Karthik Dantu[1]

***Abstract*— The RoboBee is a novel insect-scale flapping wing Micro Aerial Vehicle that is envisioned to enable exciting applications. While recent results have demonstrated full control as well as biomimetic behaviors such as perching, more complex challenges such as perception and navigation still exist. Typically, challenges in perception-based control can only be solved by experimentation. However, such fly-size MAVs are not widely available to researchers at large due to its intricate manufacturing process and limited mechanical lifetime. To facilitate the development of perception and control algorithms of insect-scale MAVs, we explore an approach of simulating flapping wing aerial vehicle dynamics on a quad-rotor. This work performs detailed analysis of the transformation of control inputs, and demonstrates feasibility by numerically simulating basic flight patterns of models of a RoboBee as well as that of a scaled quad-rotor.**

I. Introduction

Developments in wing design, aerodynamics and flapping wing control [1] are enabling a new class of tiny flying robots with flapping wings, such as the Robobee (80 mg) (Figure 1) [1][2][3][4]. Their size and flight dynamics promise to enable new applications including massively parallel operation (such as crop pollination or distributed search) as well as covert operation (such as surveillance). However, the platforms are in the early stage of their development with several challenges in sensing, control and coordination that are yet to be solved.

A primary challenge is access to such platforms for widespread experimentation. Such robots are produced in specialized labs and not easily accessible to researchers at large. Further, their nascent design process leads to manufacturing and durability challenges for large scale testing. It is hard to develop estimation and control even with access to the platform, since each robot takes about several days to assemble and is available for experimentation for limited time because of the limited mechanical lifetime of the flight mechanism. Shown in Figure 1 is an image of *RoboBee*, a flapping-wing aerial vehicle developed by the Harvard Microrobotics Lab[1].

The goal of this research is to simulate flight dynamics of a flapping wing MAV on a more widely available platform, the quad-rotor. Prior experiments have modelled the aerodynamics of robot insect flight [1] [2] [3] [4] [5] [6] [7], while others have considered perception and flight control challenges of such a robot in simulation [8] [9]. However, many challenges in perception based control can only be encountered and tackled in the real world. This is because many real-world phenomena exibit complexity that is hard to model. Examples include turbulence, sound propagation, and visual scenery. Accordingly, our goal is to provide a testing platform aimed at facilitating the development of perception and control systems targeted at insect-scale robots by simulating their behavior on a more accessible platform, a quadrotor. Our goal specifically is to take control input to a flapping wing MAV, and compute the inputs to a quadrotor that would mimic the flapping wing dynamics. We then pass this on as input to the quadrotor, to simulate flapping wing flight. While this sounds straight forward, a quad rotor is

Fig. 1. An Image of the *RoboBee* as developed at the Harvard Micro-Robotics Lab

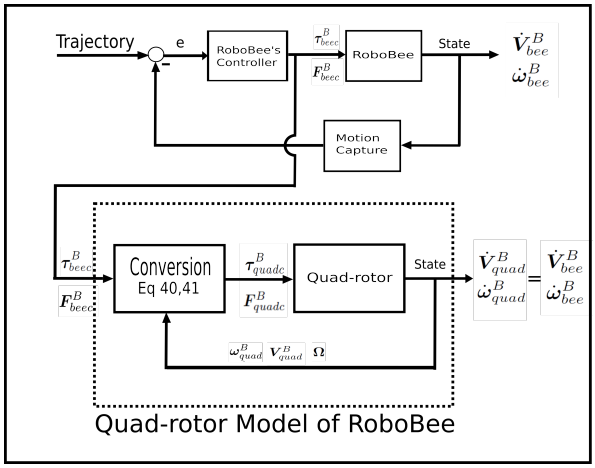

Fig. 2. We aim to achieve identical accelerations by converting a flapping wing MAV's input to a quad-rotor's input

*This work was not supported by any organization

[1]Yuyang Chen is a graduate student and Karthik Dantu is an Assistant Professor in the department of Computer Science and Engineering, University at Buffalo - State University of New York, 338 Davis Hall, Buffalo, NY 14260-2500. {yuyangch, kdantu}@buffalo.edu

[2]Sawyer B. Fuller is an Assistant Professor in the department of Mechanical Engineering, University of Washington, Seattle WA 98195 minster@uw.edu

[1]http://micro.seas.harvard.edu

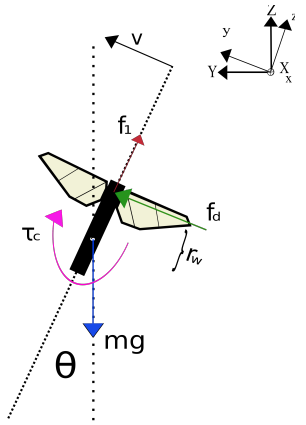

Fig. 3. Visual Representation of Flapping-wing MAV Model

intrinsically different from a flapping wing MAV. We study the flights that we can simulate and ones we cannot. We present the challenges in performing such simulation on a quadrotor, a detailed description of our modeling, simple simulation results, limits of flight simulation on a simple quad-rotor and a discussion on the limits of this work. We intend to perform experimental validation of our simulation to demonstrate the feasibility of our methodology in the future.

We must explicitly state that this paper has no notions of trajectory following. Instead, we aim to devise a system where a quad-rotor can take a RoboBee's input and produce the respective RoboBee accelerations.

II. Flight Models

In this section, we will outline both the linearized planar model and the full model for a flapping wing MAV as well as a quadrotor. For the full models, to simplify the rigid body dynamics, we assume that (a) The origin of the body fixed frame o_B coincides with the center of mass (COM) of the body, and (b) the axes of body fixed frame coincide with the body principle axes of inertia. In this case, the inertia matrix I is diagonal.

With the above assumptions, we use a generic 6 DOF rigid body dynamics model:

$$\begin{bmatrix} m\boldsymbol{I}_{3\times3} & 0_{3\times3} \\ 0_{3\times3} & \boldsymbol{I} \end{bmatrix} \begin{bmatrix} \dot{\boldsymbol{V}}^B \\ \dot{\boldsymbol{\omega}}^B \end{bmatrix} + \begin{bmatrix} \boldsymbol{\omega}^B \times (m\boldsymbol{V}^B) \\ \boldsymbol{\omega}^B \times (\boldsymbol{I}\boldsymbol{\omega}^B) \end{bmatrix} = \begin{bmatrix} \boldsymbol{F}^B \\ \boldsymbol{\tau}^B \end{bmatrix}$$

where m is the mass, $\boldsymbol{I}_{3\times3}$ is the 3×3 identity matrix, $\boldsymbol{I} = diag[\mathrm{J}_{XX}, \mathrm{J}_{YY}, \mathrm{J}_{ZZ}]$ is the inertia matrix, $\boldsymbol{V}^B = [V_x^B, V_y^B, V_z^B]^T$ is the linear velocity vector with respect to body frame, $\boldsymbol{\omega}^B = [\omega_x^B, \omega_y^B, \omega_z^B]^T$ is the angular velocity vector with respect to body frame, $\boldsymbol{F}^B$ is the total external force vector, and $\boldsymbol{\tau}^B$ is the total external torque vector. The second term on the left hand side is the *Coriolis-Centripetal* term.

A. Flapping Wing Dynamics Model

1) Linearized Planar Model: We show a previously proposed linearized planar model of a flapping wing MAV [2] for stability analysis. Assuming that the $z - axis$ torque is negligible, we can decouple the full model into two independent planar systems.

Consider the state vector $\boldsymbol{x} = [\theta, \omega, v]^T$, where θ is a scalar pitch angle, $\omega = \dot{\theta}$ an angular velocity and v is the lateral velocity (attached to body frame). As the rotational dynamics is relatively slow compared to the flapping frequency at this scale [10], this analysis only considered averaged stroke forces. A test of this vehicle flapping in a wind tunnel indicates that the drag force on the wing is nearly linear with the incident air speed (Figure II-A.1). This is the same for wind in $x-$ and $y-$ directions. So the model for aerodynamic drag for both cases is $f_d = -b_w v_w$ where b_w is the wing drag factor and v_w is the lateral velocity of the point on the airframe at the midpoint between the two wings. When the vehicle rotates at angular velocity ω, the velocity of the wings linearized around $\theta = 0$ is $v_w = -r_w\omega + v$ where r_w is the distance from the midpoint of the wings to the Center of Mass. Therefore, the force from the aerodynamic drag is $f_d = -b_w(v - r_w\omega)$, and the torque from aerodynamic drag is $\tau_d = -r_w f_d = b_w r_w v - b_w r_w^2 \omega$. Assuming the lift force f_1 approximately cancels out the weight mg, the lateral force from the inclined gravity vector relative to the body frame is equal to $-mg\sin\theta \approx -mg\theta$ (because $\theta \approx 0$). We can neglect second order cross-product terms in the generic 6 DOF rigid body model, and equate the force and torque to velocities according to $f = m\dot{v}$ and $\tau = \mathrm{J}\dot{\omega}$.

The equations of motion linearized around 0 pitch angle θ can be written as the state-space dynamical system $\dot{\boldsymbol{x}} = \boldsymbol{A}_{bee}\boldsymbol{x} + \boldsymbol{B}_{bee}\boldsymbol{u}$, with the state vector $\boldsymbol{x} = [\theta, \omega, v]^T$ expressed in body frame, and input vector $\boldsymbol{u} = [\tau_{bee}, F_{bee}]^T$. From [2]

$$\boldsymbol{A}_{bee} = \begin{bmatrix} 0 & 1 & 0 \\ 0 & -\frac{1}{\mathrm{J}_{bee}} b_w r_w^2 & \frac{1}{\mathrm{J}_{bee}} b_w r_w \\ -g & \frac{1}{m_{bee}} b_w r_w & -\frac{1}{m_{bee}} b_w \end{bmatrix} \tag{1}$$

$$\boldsymbol{B}_{bee} = \begin{bmatrix} 0 & 0 \\ \frac{1}{\mathrm{J}_{bee}} & 0 \\ 0 & \frac{1}{m_{bee}} \end{bmatrix} \tag{2}$$

2) Full Flapping Wing Dyanmics Model: [3] outlines a stroke-average model and [2] outlines the aerodynamic drag. Combining them, we have:

$$F_{thrust} = \frac{1}{2}\rho\beta C_L(\omega G(\omega))^2(V_{avg}^2 + V_{dif}^2) \tag{3}$$

$$\tau_{roll} = r_{cp}\rho\beta C_L(\omega G(\omega))^2(V_{avg}V_{dif}) \tag{4}$$

$$\tau_{pitch} \approx r_{cp}V_{off}G(0)F_{thrust} \tag{5}$$

$$\tau_{yaw} = \frac{1}{8}r_{cp}\rho\beta C_D(\omega G(\omega)V_{amp})^2(\frac{1-2k}{k-k^2}) \tag{6}$$

$$\boldsymbol{\tau}_{drag}^B = -b_w(\boldsymbol{r}_w \times \boldsymbol{V}^B + \boldsymbol{r}_w \times (\boldsymbol{\omega}^B \times \boldsymbol{r}_w)) \tag{7}$$

$$\boldsymbol{F}_{drag}^B = -b_w(\boldsymbol{V}^B + \boldsymbol{\omega}^B \times \boldsymbol{r}_w) \tag{8}$$

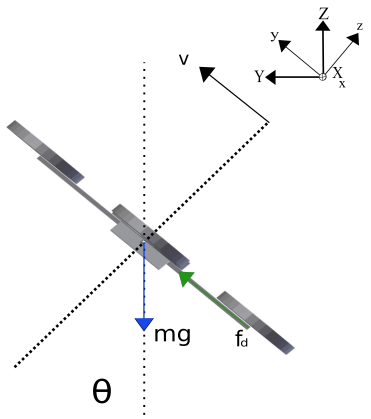

Fig. 4. Side view of Quadrotor showing gravity and wind speed in body frame

where ρ is air density, β is the wing geometric constant, C_L/C_D are the lift and drag coefficients of the the wings respectively and ω is the flapping frequency. Transfer function G is empirically determined. $V_{avg}, V_{dif}, V_{off}, k$ are the inputs that determine the input sinusoidal voltage. r_{cp} is the distance from the shoulder to the center of pressure of the wing. A detailed discussion of the parameters and variables can be found in [3]. $\boldsymbol{V}^B$ is the linear velocity vector with respect to body frame. $\boldsymbol{\omega}^B$ is the angular velocity vector with respect to body frame. $\mathbf{r}_w = [0\ 0\ r_w]^T, r_w = 9mm$ is the distance from center of mass to the shoulders. $\boldsymbol{\tau}^B_{drag}$ is the drag torque of MAV in the body frame. $\boldsymbol{F}^B_{drag}$ is the drag force of MAV in the body frame. Detailed information regarding these parameters and variables can be found in [2].

To summarize:

$$\boldsymbol{\tau}^B_{beec} = [\tau_{roll}, \tau_{pitch}, \tau_{yaw}]^T \tag{9}$$
$$\boldsymbol{F}^B_{beec} = [0, 0, F_{thrust}]^T \tag{10}$$
$$\boldsymbol{\tau}^B_{bee} = \boldsymbol{\tau}^B_{beec} + \boldsymbol{\tau}^B_{drag} \tag{11}$$
$$\boldsymbol{F}^B_{bee} = \boldsymbol{F}^B_{beec} + \boldsymbol{F}^B_{beeg} + \boldsymbol{F}^B_{drag} \tag{12}$$

where $\boldsymbol{\tau}^B_{bee}$ and $\boldsymbol{F}^B_{bee}$ are terms on the right hand side of the generic 6 DOF rigid body dynamic model. They determine $\dot{\boldsymbol{V}}^B_{bee}$ and $\dot{\boldsymbol{\omega}}^B_{bee}$.

3) RoboBee Actuator Delay Characteristics: In [1], in order to achieve full control, the author uses the following transfer function to approximate the RoboBee's muscle-thorax-wings system's transient response.

$$\frac{X}{V} = \frac{A}{m_{eq}(s)^2 + b_{eq}(s) + k_{eq}} \tag{13}$$

where m_{eq}, b_{eq}, k_{eq} are the equivalent mass, equivalent damper coefficient and equivalent spring constant respectively of the piezoelectric actuators. X is the displacement of the piezoelectric actuator and V is the voltage applied. Details can be found in [3].

B. Quad-rotor Dynamics Model

1) Quad-rotor Linearized Planar Model: We will present a planar quad-rotor model (Figure 4) for stability analysis in Section III. If $z-$ torque and τ^B_{gyro} is negligibly small, we can decouple the quad-rotor into two planar systems. Prior research [11], [12], [13], [14], [15] acknowledges that a quad-rotor experiences drag force that scales linearly with lateral velocity attached to the body frame.

$$f_d = -uv$$

One could use onboard IMU readings to estimate the coefficient u [11]. Assuming the lift force f_1 approximately cancels out the weight mg, the lateral force from the inclined gravity vector relative to the body frame is equal to $-mg\sin\theta \approx -mg\theta$. We can neglect the second order cross-product terms from the generic 6 DOF rigid body model, and equate the force and torque to velocities according to $f = m\dot{v}$ and $\tau = \mathrm{J}\dot{\omega}$. The equation of motion linearized around 0 pitch angle θ can be written as a state-space dynamical system $\dot{\boldsymbol{x}} = \boldsymbol{A}_{quad}\boldsymbol{x} + \boldsymbol{B}_{quad}\boldsymbol{u}$, with the state vector $\boldsymbol{x} = [\theta, \omega, v]^T$ expressed in the body coordinate, and the input vector $\boldsymbol{u} = [\tau_{quad}, F_{quad}]^T$. Where

$$\boldsymbol{A}_{quad} = \begin{bmatrix} 0 & 1 & 0 \\ 0 & 0 & 0 \\ -g & 0 & -\frac{1}{m_{quad}}u \end{bmatrix} \tag{14}$$

$$\boldsymbol{B}_{quad} = \begin{bmatrix} 0 & 0 \\ \frac{1}{\mathrm{J}_{quad}} & 0 \\ 0 & \frac{1}{m_{quad}} \end{bmatrix} \tag{15}$$

2) Quad-rotor Full Model: [16] outlines the quad-rotor model:

$$F_{thrust} = b(\Omega_1^2 + \Omega_2^2 + \Omega_3^2 + \Omega_4^2) \tag{16}$$
$$\tau_{roll} = lb(-\Omega_2^2 + \Omega_4^2) \tag{17}$$
$$\tau_{pitch} = lb(-\Omega_1^2 + \Omega_3^2) \tag{18}$$
$$\tau_{yaw} = d(-\Omega_1^2 + \Omega_2^2 - \Omega_3^2 + \Omega_4^2) \tag{19}$$
$$\boldsymbol{\tau}^B_{gyro} = J_{TP}\begin{bmatrix} -\omega^B_x(-\Omega_1 + \Omega_2 - \Omega_3 + \Omega_4) \\ \omega^B_y(-\Omega_1 + \Omega_2 - \Omega_3 + \Omega_4) \\ 0 \end{bmatrix} \tag{20}$$
$$\boldsymbol{F}^B_{drag} = -u\boldsymbol{V}^B \tag{21}$$

where Ω_n is the n_{th} propeller's angular speed in rad/s, b is the propeller thrust factor, l is the distance from propeller to the center of mass, d is the propeller drag factor and $\boldsymbol{\tau}^B_{gyro}$ is the gyroscopic torque that arise from propeller speed imbalance. For more details about these parameters and variables refer to [16].

To summarize:

$$\boldsymbol{\tau}^B_{quadc} = [\tau_{roll}, \tau_{pitch}, \tau_{yaw}]^T \tag{22}$$
$$\boldsymbol{F}^B_{quadc} = [0, 0, F_{thrust}]^T \tag{23}$$
$$\boldsymbol{\tau}^B_{quad} = \boldsymbol{\tau}^B_{quadc} + \boldsymbol{\tau}^B_{gyro} \tag{24}$$
$$\boldsymbol{F}^B_{quad} = \boldsymbol{F}^B_{quadc} + \boldsymbol{F}^B_{quadg} + \boldsymbol{F}^B_{drag} \tag{25}$$

TABLE 1
TABLE OF ROBOBEE (TOP) AND QUAD-ROTOR (BOTTOM) PARAMETERS

Parameter	Unit	Description
ρ	kg/m^3	Air density
β		Wing geometric constant
C_L		Lift coefficient of the wings
C_D		Drag coefficient of the wings
r_{cp}	m	Shoulder to wing center of pressure
r_w	m	Center of mass to the shoulders
b_w	N/ms^{-1}	Lateral drag factor of the wings
m_{eq}	m	Equivalent mass of piezo actuators
b_{eq}	m	Equivalent damper factor of piezo actuator
k_{eq}	m	Equivalent spring constant of piezo actuator
l	m	CM of quadrotor to the center of props
b	Ns^2	prop thrust factor
d	Nms^2	Prop drag factor
u	N/ms^{-1}	Lateral drag factor
KE	V s /rad	Electrical motor constant
KM	V s /rad	Mechanical motor constant
η		Gear box coefficient
N		Gear box reduction ratio
R	Ω	Motor Resistance
J_P	Nms^2	Prop axis moment of inertia
J_M	Nms^2	Motor axis moment of inertia
J_{TP}	Nms^2	Total prop axis moment of inertia

where $\boldsymbol{\tau}^B_{quad}$ and $\boldsymbol{F}^B_{quad}$ are terms on the right hand side of the generic 6 DOF rigid body dynamic model. They determine $\dot{\boldsymbol{V}}^B_{quad}$ and $\dot{\boldsymbol{\omega}}^B_{quad}$.

3) Quad-rotor Motor Delay Characteristics: The following equation takes into account motor dynamics and shows the relationship between propeller's speed and motor's input voltage.

$$(J_P + \eta N^2 J_M)\dot{\boldsymbol{\Omega}} = -\frac{K_E K_M}{R}\eta N^2 \boldsymbol{\Omega} - d\boldsymbol{\Omega}^2 + \frac{K_M}{R}\eta N \mathbf{v} \tag{26}$$

We summarize the parameters used and their descriptions in TABLE 1 for reference. During experimental validation, parameters in the TABLE 1 will need to be determined according to methods introduced in [16].

III. OVERVIEW OF OUR APPROACH

This section discusses our approach to simulating flight dynamics (Figure 2). For this discussion, we assume that flapping wing flight is being simulated on a bitcraze crazyflie 2.0 quadrotor[2] that is commercially available for purchase. This quadrotor is about 10cm across, weighs 27g and has enough computing and sensing to perform interesting sensing/navigation flight experiments.

A. Resolving Size Differences

Perhaps the most pronounced difference between a 80mg MAV and a 27g quadrotor is the difference in mass and inertia matrix. A direct consequence is that the MAV experiences different Coriolis-Centripetal effects compared to the quad-rotor. In addition, the two vehicles experience different aerodynamic drag. Thus, if one simply experiments on a quad-rotor without any kind of force and torque scaling, these differences are not compensated for.

[2] https://www.bitcraze.io/crazyflie-2/

For the rest of this discussion, we assume the proposed MAV and quad-rotor model accurately describe the vehicles' dynamics. And one would rely on controller robustness to correct model error.

We can show that under the assumption above, through the scaling of force and torque input, it is theoretically possible to achieve identical motion under the same initial conditions on two different vehicles with different masses and inertia matrices if the actuators of the larger vehicle has enough output capacity.

The analysis below follows the generic 6 DOF dynamic model described in II. The goal is to equalize linear and rotational acceleration in the body frame, so the states which contain zero and first order pose information are identical in the time domain:

$$\dot{\boldsymbol{V}}^B_{quad} = \dot{\boldsymbol{V}}^B_{bee} \tag{27}$$

$$\dot{\boldsymbol{\omega}}^B_{quad} = \dot{\boldsymbol{\omega}}^B_{bee} \tag{28}$$

It can be shown that, if the first order state is identical ,where $\boldsymbol{\omega}^B = \boldsymbol{\omega}^B_{quad} = \boldsymbol{\omega}^B_{bee}$, $\boldsymbol{V}^B = \boldsymbol{V}^B_{quad} = \boldsymbol{V}^B_{bee}$, then we can achieve Equation 27 by:

$$\boldsymbol{F}^B_{quad} = \frac{m_{quad}}{m_{bee}}\boldsymbol{F}^B_{bee} \tag{29}$$

regardless of the Coriolis-Centripetal term. This can be shown by

$$m_{bee}\dot{\boldsymbol{V}}^B_{bee} + \boldsymbol{\omega}^B \times (m_{bee}\boldsymbol{V}^B) = \boldsymbol{F}^B_{bee} \tag{30}$$

$$m_{quad}\dot{\boldsymbol{V}}^B_{quad} + \boldsymbol{\omega}^B \times (m_{quad}\boldsymbol{V}^B) = \boldsymbol{F}^B_{quad} \tag{31}$$

$$\dot{\boldsymbol{V}}^B_{bee} = \frac{\boldsymbol{F}^B_{bee}}{m_{bee}} - \boldsymbol{\omega}^B \times (\boldsymbol{V}^B) \tag{32}$$

$$\dot{\boldsymbol{V}}^B_{quad} = \frac{\boldsymbol{F}^B_{quad}}{m_{quad}} - \boldsymbol{\omega}^B \times (\boldsymbol{V}^B) \tag{33}$$

Combining Equation 29 and Equation 33:

$$\dot{\boldsymbol{V}}^B_{quad} = \frac{m_{quad}\boldsymbol{F}^B_{bee}}{m_{quad}m_{bee}} - \boldsymbol{\omega}^B \times (\boldsymbol{V}^B) = \dot{\boldsymbol{V}}^B_{bee} \tag{34}$$

Similarly, we can achieve Equation 28 by finding a specific $\boldsymbol{\tau}^B_{quad}$ according to the Coriolis-Centripetal term and $\boldsymbol{\tau}^B_{bee}$, we again assume the equality of states $\boldsymbol{\omega}^B = \boldsymbol{\omega}^B_{quad} = \boldsymbol{\omega}^B_{bee}$

$$\dot{\boldsymbol{\omega}}^B_{bee} = \boldsymbol{I}^{-1}_{bee}\boldsymbol{\tau}^B_{bee} - \boldsymbol{I}^{-1}_{bee}\boldsymbol{\omega}^B \times (\boldsymbol{I}_{bee}\boldsymbol{\omega}^B) \tag{35}$$

$$\dot{\boldsymbol{\omega}}^B_{quad} = \boldsymbol{I}^{-1}_{quad}\boldsymbol{\tau}^B_{quad} - \boldsymbol{I}^{-1}_{quad}\boldsymbol{\omega}^B \times (\boldsymbol{I}_{quad}\boldsymbol{\omega}^B) \tag{36}$$

$$\dot{\boldsymbol{\omega}}^B_{quad} = \dot{\boldsymbol{\omega}}^B_{bee} \tag{37}$$

$$\boldsymbol{I}^{-1}_{quad}\boldsymbol{\tau}^B_{quad} - \boldsymbol{I}^{-1}_{quad}\boldsymbol{\omega}^B \times (\boldsymbol{I}_{quad}\boldsymbol{\omega}^B) = \boldsymbol{I}^{-1}_{bee}\boldsymbol{\tau}^B_{bee} - \boldsymbol{I}^{-1}_{bee}\boldsymbol{\omega}^B \times (\boldsymbol{I}_{bee}\boldsymbol{\omega}^B) \tag{38}$$

$$\boldsymbol{\tau}^B_{quad} = \boldsymbol{I}_{quad}\boldsymbol{I}^{-1}_{bee}\boldsymbol{\tau}^B_{bee} - \boldsymbol{I}_{quad}\boldsymbol{I}^{-1}_{bee}\boldsymbol{\omega}^B \times (\boldsymbol{I}_{bee}\boldsymbol{\omega}^B) + \boldsymbol{\omega}^B \times (\boldsymbol{I}_{quad}\boldsymbol{\omega}^B) \tag{39}$$

Strictly speaking, the $\boldsymbol{\omega}^B$ in the last two terms belong to two different vehicles respectively. In our method, we will use $\boldsymbol{\omega}^B = \boldsymbol{\omega}^B_{quad}$, in other words $\boldsymbol{\omega}^B_{quad} = \boldsymbol{\omega}^B_{bee}$, because we assume the states are nearly identical. Thus this compensation would not required any information other than the information from the quad-rotor's own states.

from Equation 39, we can also show that when $\mathsf{J}_{XX} = \mathsf{J}_{YY}$and $\omega_z = 0$ for both quad and bee, we can replace Equation 39 with simply $\boldsymbol{\tau}^B_{quad} = \boldsymbol{I}_{quad}\boldsymbol{I}^{-1}_{bee}\boldsymbol{\tau}^B_{bee}$.

To summarize, from the scaling of Equation 29 and Equation 39, we can achieve the same force Equation 27 and torque Equation 28 resulting in the equality of linear and angular accelerations respectively.

B. Resolving Dynamic Torque Difference

A RoboBee's Center of Mass hangs below its wings. When the RoboBee is performing flapping wing vehicle maneuvers through the air, its wings experience aerodynamic drag. Thus a RoboBee experiences drag force opposite to the linear direction of travel, and drag torque proportional to angular and linear velocity. Thus, it experiences pendulum like dynamics. Such dynamics can be described by the aerodynamic drag, shown in Equations 7,8. For a more detailed discussion, one can refer to [2].

The effect of aerodynamic drag is unique to RoboBee. A quad-rotor does not experience significant drag torque in the roll and pitch axes. Instead, a quad-rotor experiences gyroscopic effects produced by propellers rotation. Since two of the propellers rotate clockwise and the other two counterclockwise, there is an overall imbalance when the algebraic sum of the rotors speed is not equal to zero. If, in addition, the roll or pitch rates are also different than zero, the quad-rotor experiences a gyroscopic torque according to Equation 20. For the details, one can refer to [16]. Therefore, we must compensate for such differences between the dynamic torques so the quadrotor behaves like the RoboBee.

The method to compensate for dynamic drag is straightforward. From Equations 7, 20, 39, to achieve the equality of angular accelerations, the following is a mapping from $\boldsymbol{\tau}^B_{beec}$ to $\boldsymbol{\tau}^B_{quadc}$:

$$\begin{aligned}\boldsymbol{\tau}^B_{quadc} = {} & \boldsymbol{I}_{quad}\boldsymbol{I}^{-1}_{bee}\boldsymbol{\tau}^B_{beec} \\ & + \boldsymbol{I}_{quad}\boldsymbol{I}^{-1}_{bee}(-b_w(\boldsymbol{r}_w \times \boldsymbol{V}^B + \boldsymbol{r}_w \times (\boldsymbol{\omega}^B \times \boldsymbol{r}_w))) \\ & - \boldsymbol{I}_{quad}\boldsymbol{I}^{-1}_{bee}\boldsymbol{\omega}^B \times (\boldsymbol{I}_{bee}\boldsymbol{\omega}^B) + \boldsymbol{\omega}^B \times (\boldsymbol{I}_{quad}\boldsymbol{\omega}^B) \\ & - J_{TP}\begin{bmatrix} -\omega^B_x(-\Omega_1 + \Omega_2 - \Omega_3 + \Omega_4) \\ \omega^B_y(-\Omega_1 + \Omega_2 - \Omega_3 + \Omega_4) \\ 0 \end{bmatrix}\end{aligned} \tag{40}$$

Because of the non-holononmic nature of the quad-rotor, it can only compensate for the force difference in the z-direction. Therefore, according to Equation 29, we scaled up the control:

$$\boldsymbol{F}^B_{quadc} = \frac{m_{quad}}{m_{bee}}\boldsymbol{F}^B_{beec} \tag{41}$$

C. Attitude Stability Analysis of the RoboBee and the Quadrotor

If the Quad-rotor is calibrated to function as a hovering confirmation vehicle for the RoboBee, then it should pose a equivalent if not a slightly harder hovering control challenge. The central idea of this section is that by scaling the terms in Equation 40 right hand side second term, we can make the quad-rotor to pose an equivalent hovering control challenge.

We first look at the RoboBee's linearized state-space model (Equations 1, 2) and their stability, as outlined in [2]. The dynamics are asymptotically stable if the eigenvalues of the matrix $\boldsymbol{A}_{bee}$ all have negative real part. In [2], the authors use additional control damping $\tau_c = -k_d\omega$ to stabilize the RoboBee. Thus $\tau_{bee} = \tau_c + \tau_d$. and $A_{bee,22}$ becomes $-(\frac{1}{\mathsf{J}_{bee}}b_w r_w^2 + k_d)$. By using the Routh-Hurtwitz criterion, they determined the minimal k_d, which is $\underline{k_d}$ needed to stabilize $\boldsymbol{A}_{bee}$ is 0.9×10^{-7}, for both $xz-$ and $yz-$ planes. Also, the $\underline{k_d}$ determined from the planar model is applicable to the full model.

By Equations 40, 41 we can achieve the mapping described in Equations 29, 39. If we ignore the the non-holonomic nature of the Quadrotor, it can be shown that the Quadrotor's linearized planar model is identical to that of the RoboBee. However, because a quadrotor is non-holonomic, it is not able to compensate for the drag force induced by angular or linear velocity. To show the above claim, we make a linearize planar mapped quad-rotor model without the consideration of propeller gyroscopic torque. We take Equation 40 and throw away the last two terms in the right-hand side (the third term disappear in a linearize model). Take this modified Equations 40 and 41 into Equations 24, 25. Then take Equations 24, 25 into the generic 6 DOF rigid body dynamic model, take its planar version. The quad-rotor's new planar models become:

$$\boldsymbol{A}_{quad,mapped} = \begin{bmatrix} 0 & 1 & 0 \\ 0 & -\frac{1}{\mathsf{J}_{bee}}b_w r_w^2 & \frac{1}{\mathsf{J}_{bee}}b_w r_w \\ -g & 0 & -\frac{1}{m_{quad}}u \end{bmatrix} \tag{42}$$

$$\boldsymbol{B}_{quad,mapped} = \begin{bmatrix} 0 & 0 \\ \frac{1}{\mathsf{J}_{bee}} & 0 \\ 0 & \frac{1}{m_{bee}} \end{bmatrix} \tag{43}$$

to see why in $\boldsymbol{B}_{quad,mapped}$ the terms change from $\frac{1}{\mathsf{J}_{quad}}$ and $\frac{1}{m_{quad}}$ to $\frac{1}{\mathsf{J}_{bee}}$ and $\frac{1}{m_{bee}}$ respectively, and in $\boldsymbol{A}_{quad,mapped}$ the second row is modified to be identical to that of $\boldsymbol{A}_{bee}$. First refer to Equation 40, right hand side first term. $\boldsymbol{\tau}^B_{beec}$ is scaled by $\boldsymbol{I}_{quad}\boldsymbol{I}^{-1}_{bee}$. Thus in the planar version,

$\tau_{quadc} = \frac{\mathrm{J}_{quad}}{\mathrm{J}_{bee}}\tau_{beec}$. Now, consider Equation 40 right hand side second term. The part inside the bracket is converted to $b_w r_w v - b_w r_w^2 \omega$ in the planar model (which is τ_d). this is also scaled by $\frac{\mathrm{J}_{quad}}{\mathrm{J}_{bee}}$. Overall $\tau_{quad} = \frac{\mathrm{J}_{quad}}{\mathrm{J}_{bee}}(\tau_{beec} + b_w r_w v - b_w r_w^2 \omega)$. Thus in the planar model $\dot{\omega}_{quad} = \frac{\tau_{quad}}{\mathrm{J}_{quad}} = \frac{1}{\mathrm{J}_{bee}}(\tau_{beec} + b_w r_w v - b_w r_w^2 \omega)$. Which is why $\boldsymbol{B}_{quad,mapped}$ and $\boldsymbol{A}_{quad,mapped}$ appear in such format.

By the same reasoning from Routh-Hurtwitz criterion, for $\boldsymbol{A}_{bee}$, increase the magnitude of $A_{bee,23}$ and $A_{bee,32}$, destabilizes the system. This means that linear velocity induced torque and angular velocity induced force, respectively, destabilize the system. On the other hand, increasing the magnitudes of $A_{bee,22}$ and $A_{bee,33}$, stabilizes the system. This means that angular velocity induced drag torque and linear velocity induced drag force stabilize the system. this is true because they are in the opposite direction from the states that induce them.

We write $-\frac{1}{m_{quad}}u = -\zeta\frac{1}{m_{bee}}b_w$. so that $\zeta = \frac{-\frac{1}{m_{quad}}u}{-\frac{1}{m_{bee}}b_w}$. ζ has the following physical meaning: *ratio of lateral drag acceleration induced under the same lateral velocity*. It can be shown that if $\zeta = 1$, $\boldsymbol{A}_{quad,mapped}$ is a little easier to stabilize because of the missing $A_{bee,32}$ term. However, we can show that in Equation 40, right hand side second term, if we compensate the linear velocity induced drag torque or angular velocity induced drag torque slightly differently, we can make the quad-rotor an equivalent, if not a harder vehicle to stabilize. To be specific, we reduce the magnitude of $A_{quad,mapped,22}$ (which stabilizes the system) and increase the magnitude of $A_{quad,mapped,23}$ (which destabilizes the system).

From the view point of angular velocity damping, it can be shown that if $\zeta = 1$, one need to only scale up $A_{quad,mapped,23}$ by a factor of $\beta = 1.1481$, or alternatively, scale $A_{quad,mapped,22}$ by a factor of $\alpha = 0.4174$, so the minimum angular velocity damping to stabilize this vehicle is the same as $\underline{k_d}$. Thus this quadrotor is quantitatively equally hard to use angular velocity damping to stabilize compared to a RoboBee.

The factors of scaling α, β, according to ζ can be determined through Roth-Hurtwitz criterion by solving for the same $\underline{k_d}$. Also, if the quadrotor is calibrated as a hovering confirmation vehicle then its ability to mimic the same trajectory of the RoboBee is degraded.

D. Resolving Actuator Transient Response Difference

Comparing the piezoelectric actuators of RoboBee with the brush motors of a quadrotor, one can find very different transient responses. For the quadrotors, the individual motor's response equation can be found in Equation 26. We linearize this equation around a hovering operation point Ω_0:

$$(J_P + \eta N^2 J_M)\dot{\mathbf{\Omega}} = -\frac{K_E K_M}{R}\eta N^2 \mathbf{\Omega} - d\Omega_0 \mathbf{\Omega} + \frac{K_M}{R}\eta N \mathbf{v} \tag{44}$$

where $\mathbf{\Omega}$ is the propeller angular velocity in Rad/s, $\mathbf{v}$ is the input voltage in volts.

For the RoboBee's muscle-thorax-wings system's transient response, the approximation can be found in Equation 13.

To define the transient responses more precisely, we will present two different actuator groups with the following state-space representation.

For RoboBee, $\dot{\boldsymbol{x}} = \boldsymbol{A}\boldsymbol{x} + \boldsymbol{B}\boldsymbol{u}$: .

$$\begin{bmatrix} \dot{x_1} \\ \dot{x_2} \\ \dot{x_3} \\ \dot{x_4} \end{bmatrix} = \begin{bmatrix} & 1 & & \\ -\frac{k_{eq}}{m_{eq}} & -\frac{b_{eq}}{m_{eq}} & & \\ & & & 1 \\ & & -\frac{k_{eq}}{m_{eq}} & -\frac{b_{eq}}{m_{eq}} \end{bmatrix} \begin{bmatrix} x_1 \\ x_2 \\ x_3 \\ x_4 \end{bmatrix} + \begin{bmatrix} 0 & 0 \\ \frac{A}{m_{eq}} & 0 \\ 0 & 0 \\ 0 & \frac{A}{m_{eq}} \end{bmatrix} \begin{bmatrix} v_1 \\ v_2 \end{bmatrix}$$

For the quadrotor,$\dot{\boldsymbol{x}} = \boldsymbol{A}\boldsymbol{x} + \boldsymbol{B}\boldsymbol{u}$:

$$\begin{bmatrix} \dot{\Omega}_1 \\ \dot{\Omega}_2 \\ \dot{\Omega}_3 \\ \dot{\Omega}_4 \end{bmatrix} = \begin{bmatrix} \alpha & & & \\ & \alpha & & \\ & & \alpha & \\ & & & \alpha \end{bmatrix} \begin{bmatrix} \Omega_1 \\ \Omega_2 \\ \Omega_3 \\ \Omega_4 \end{bmatrix} + \begin{bmatrix} \beta & & & \\ & \beta & & \\ & & \beta & \\ & & & \beta \end{bmatrix} \begin{bmatrix} v_1 \\ v_2 \\ v_3 \\ v_4 \end{bmatrix}$$

where α, β are scalars, $\alpha = (\frac{K_E K_M}{R}\eta N^2 - d\Omega_0)/(J_P + \eta N^2 J_M)$, $\beta = (\frac{K_M}{R}\eta N)/(J_P + \eta N^2 J_M)$. In theory, it is possible through state feed back to place the poles of quadrotor motor state-space to be the same as the poles of Robobee Piezoelectric actuator's. We first need to install optical RPM readers on the quadrotor, to provide feedback about the propellers' angular velocity.

Then, through feedback , where $\boldsymbol{u} = \boldsymbol{r} - \boldsymbol{K}\boldsymbol{x}$, the quadrotor's motor group state-space becomes:

$$\dot{\boldsymbol{x}} = (\boldsymbol{A} - \boldsymbol{B}\boldsymbol{K})\boldsymbol{x} + \boldsymbol{B}\boldsymbol{r} \tag{45}$$

$\boldsymbol{K}$ is obtained by solving for the same real parts of the eigenvalues of quadrotor and Robobee's state space. Although we are not sure about the output equation $\boldsymbol{y} = \boldsymbol{C}\boldsymbol{x}$ for the RoboBee, we know the DC gain in relation to input as described in [3].

Thus $\boldsymbol{r}$ can be determined through scaling described in Equations 40, 41 and the DC gain of RobeBee and quadrotor's actuator group.

More precisely, quadrotor's desired steady state U_1, U_2, U_3, U_4 will first be calculated through Equations 22, 23 in relationship to RoboBee's input signal. Thus $\boldsymbol{y}_{ss} = \boldsymbol{U}$. Through this relationship: $\boldsymbol{y}_{ss} = -\boldsymbol{C}(\boldsymbol{A} - \boldsymbol{B}\boldsymbol{K})^{-1}\boldsymbol{B}\boldsymbol{r}$ one can determine $\boldsymbol{r}$

In experimental validation, it might not be possible to achieve the desired pole-placements because of the limitation of the quadtrotor's power supply. While the above actuator latency analysis was not incorporated into the simulations below, we plan to tackle this in future work.

E. Specification of Valid Range of Operation of Simulated Dynamics

A RoboBee is extremely agile rotationally, due to its extremely low moment of inertia among the principle axes. According to [3], a RoboBee (without additional sensors attached) is able to produce maximum torque of $3mm \times mN$ in the roll direction. According to [2], a RoboBee's $x-$ and $y-$ axes inertia are $1.4 \times 10^{-9} kgm^2$. Therefore a RoboBee is able to produce the maximum rotational acceleration of

$2112.67 rad/s^2$ in the roll direction. The number is slightly smaller in the pitch direction. A quad-rotor, at the scale of Crazyflie 2.0, is able to produce the maximum roll or pitch angular acceleration of $537 rad/s^2$ [17] [18]. This is about 25% of a RoboBee's capability. If additional sensors are attached, the RoboBee's moments of inertia among the principle axes will increase. For example if we compare a Crazyflie to the RoboBee with an oceli attached [2], the performance percentage increases to 32.22%. The quad-rotor would require about 33.33% of the RoboBee's roll torque capability. This can be shown from The flight data of the RoboBee's hovering [1] and take off [2]. The thrust to weight ratio of a Robobee is approximately 2 [3] while that of a Crazyflie is approximately 2.28. Therefore a Crazyflie is at 114% thrust capability.

F. The Summary of Our Approach to Compensate for the Quad-rotor

- Take the control inputs from a RoboBee controller and convert them into quad-rotor inputs by Equations 40, 41.
- Secondly, use state-feedback to make the motor's transient response to be as close to that of the MAV's actuator transient response as possible (according to III-D)
- Choose small quad-rotors with a favorable ζ. Ideally, this ζ should be as close to 1 as possible. The quad-rotor should also have the adequate maximum torque capability as described in III-E.

IV. Simulation

We record the simulated flight data of three vehicles, a flapping wing MAV, a quad-rotor calibrated to mimic its motion and a uncalibrated quad-rotor. We labeled the flapping wing MAV's data as "RoboBee", the calibrated quad-rotor as "QuadroBee" and the uncalibrated quad-rotor as "Quadrotor". Two identical LQR controllers (calibrated for the RoboBee) are used for the RoboBee and the QuadroBee's control. This controller's command is scaled for the Quadrobee according to Equations 40, 41. A separate LQR controller (calibrated for the normal quad-rotor) is used for the uncompensated quad-rotor's control. All the respective penalties among the $\boldsymbol{Q}$ matrices are equivalent between the two LQR controllers. We will use $\boldsymbol{q} = [\theta_x, \theta_y, \theta_z, \omega_x^B, \omega_y^B, \omega_z^B, X, Y, Z, V_x^B, V_y^B, V_z^B]^T$ to represent the vehicles' states where angles $\theta_x, \theta_y, \theta_z$ and displacements X, Y, Z are referencing to the world frame. The rest of the states are referencing to the body frame. All three vehicles are given the initial states $\boldsymbol{q}_0 = [.08, -.08, 0, -.1, 0, 1, .15, -.15, .01, .1, -.3, 0]^T$ and the following way points:

$$\boldsymbol{q}_1 = [0, 0, 0, 0, 0, 0, -0.15, -0.15, .2, 0, 0, 0]^T$$
$$\boldsymbol{q}_2 = [0, 0, 0, 0, 0, 0, -0.15, 0.15, .3, 0, 0, 0]^T$$
$$\boldsymbol{q}_3 = [0, 0, 0, 0, 0, 0, 0.15, 0.15, .4, 0, 0, 0]^T$$
$$\boldsymbol{q}_4 = [0, 0, 0, 0, 0, 0, 0.15, -0.15, .5, 0, 0, 0]^T$$

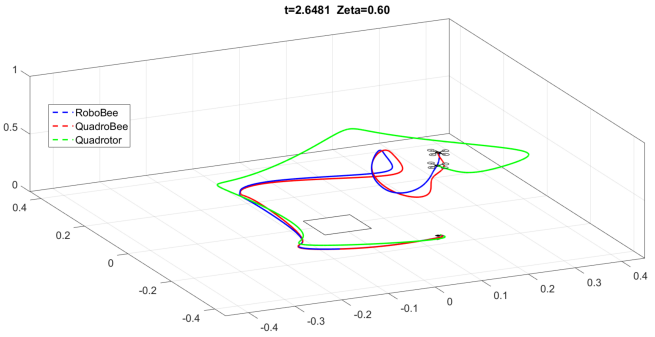

Fig. 5. Both the RoboBee and the QuadroBee (quadrotor compensated with our control scaling) uses the same altitude controller and LQR attitude controller. The uncompensated quad-rotor uses a separate LQR controller with the same state penalty $\boldsymbol{Q}$ matrix. The plot shows the compensated quad-rotor has a much similar trajectory comparing to that of the RoboBee.

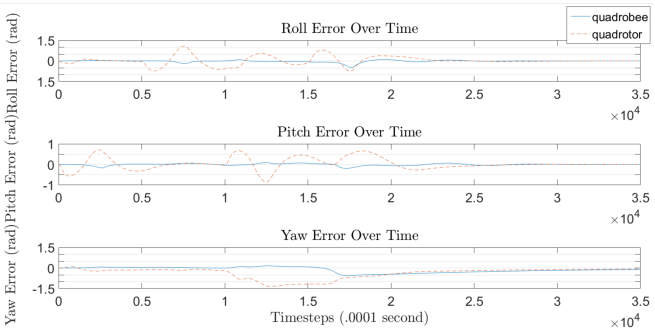

Fig. 6. Attitude error of the quad-rotors, referencing the RoboBee

which forms a square trajectory with increasing altitude. All the vehicles starts out with $\boldsymbol{q}_1$ as the targeted way point, then iterate for the next way point after each $500ms$. ζ is important for trajectory similarity since we can not compensate for the lateral drag force with motors. When $\zeta = 1$ the trajectories among the RoboBee and the compensated quad-rotor (QuadroBee) is near identical. According to [11], a $1kg$ quad-rotor has $\zeta = 0.1555$, a lighter vehicle such as a Crazyflie would have a more favorable ζ. We think the assumption that this ζ fall between .1555 and 1 is relatively safe to make. This ζ can be more precisely determined with a motion capturing system and an IMU [11]. We used $\zeta = 0.6$ in the following simulation. The video is also shown in the supplement. The following are the simulation results without considerations of the actuators' delay. The trajectories are visualized in Figure 5 and the state error are shown in Figure 6, 7

To show how ζ influences the trajectory error, we simulated the QuadroBee and RoboBee fights for the same trajectory under different ζ. We listed two graphs (Figure 8, 9) that shows average states error vs ζ. The state errors diminish when ζ approaches 1.

V. Discussion and Conclusions

This paper shows a technique that enables quad-rotors to simulate motion of a flapping wing MAV by converting the input of a flapping wing MAV into the input of a quad-rotor and compensating for scale and dynamics. We simulated the flights of a flapping wing MAV and a quad-rotor with such

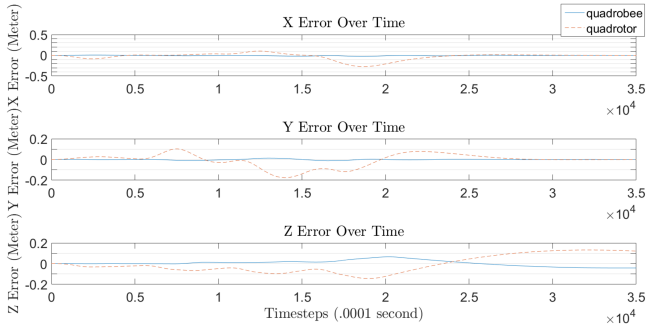

Fig. 7. Position error of the quad-rotors, referencing the RoboBee

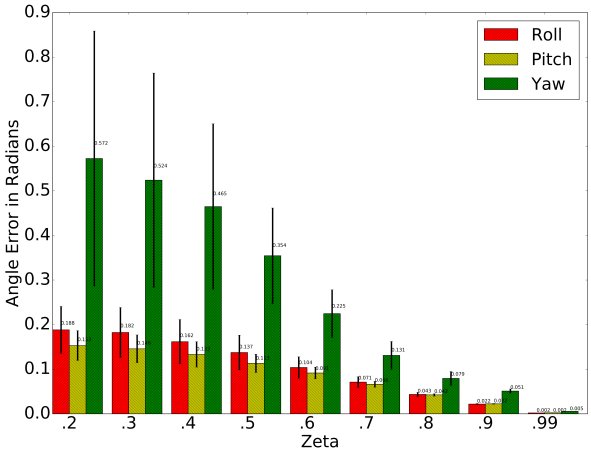

Fig. 8. Compensated quad-rotors' attitude error over time versus zeta, referencing the RoboBee. We show the mean and variance.

converted input. The results suggest that trajectory error is minimal, especially if the quad-rotor has similar acceleration induced by the lateral drag as the flapping wing MAV. Our results suggest that the smaller size quad-rotors, which have favorable ζ and maximum torque capability, are ideal for such simulation. The scope of this work is limited to a noiseless simulated environment and the our simulations do not consider actuator delays. Additionally, this work is perform with the idealized model of the vehicles. Modeling error on both the Robobee and Quadrotor will make Quadrobee behave differently than the robobee. We intend to further this investigation by considering actuator delay, sensor/input noise and model inaccuracy in the future work. We also intend to experimentally validate this simulation by comparing actual RoboBee flight as well as small quadrotor flight with our compensation.

REFERENCES

[1] K. Y. Ma, P. Chirarattananon, S. B. Fuller, and R. J. Wood, "Controlled flight of a biologically inspired, insect-scale robot," *Science*, vol. 340, no. 6132, pp. 603–607, 2013.

[2] S. B. Fuller, M. Karpelson, A. Censi, K. Y. Ma, and R. J. Wood, "Controlling free flight of a robotic fly using an onboard vision sensor inspired by insect ocelli," *Journal of The Royal Society Interface*, vol. 11, no. 97, p. 20140281, 2014.

[3] K. Y. Ma, S. M. Felton, and R. J. Wood, "Design, fabrication, and modeling of the split actuator microrobotic bee," in *Intelligent Robots and Systems (IROS), 2012 IEEE/RSJ International Conference on*. IEEE, 2012, pp. 1133–1140.

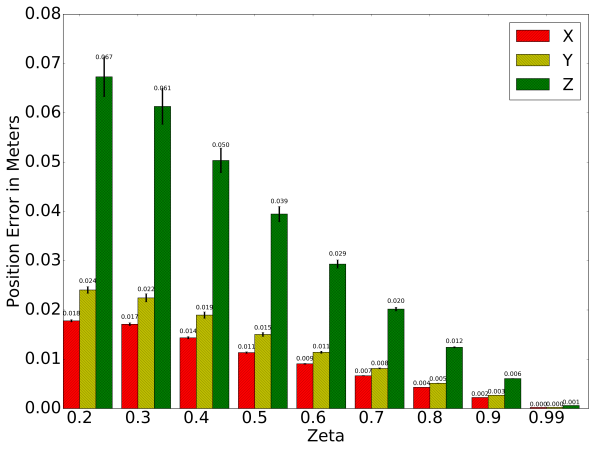

Fig. 9. Compensated quad-rotors' position error over time versus zeta, referencing the RoboBee. We show the mean and variance.

[4] R. J. Wood, "The first takeoff of a biologically inspired at-scale robotic insect," *IEEE transactions on robotics*, vol. 24, no. 2, pp. 341–347, 2008.

[5] Y. Chen, N. Gravish, A. L. Desbiens, R. Malka, and R. J. Wood, "Experimental and computational studies of the aerodynamic performance of a flapping and passively rotating insect wing," *Journal of Fluid Mechanics*, vol. 791, pp. 1–33, 2016.

[6] P. Chirarattananon, K. Y. Ma, and R. J. Wood, "Adaptive control of a millimeter-scale flapping-wing robot," *Bioinspiration & biomimetics*, vol. 9, no. 2, p. 025004, 2014.

[7] J. Whitney and R. Wood, "Aeromechanics of passive rotation in flapping flight," *Journal of Fluid Mechanics*, vol. 660, pp. 197–220, 2010.

[8] T. S. Clawson, S. Ferrari, S. B. Fuller, and R. J. Wood, "Spiking neural network (snn) control of a flapping insect-scale robot," in *Decision and Control (CDC), 2016 IEEE 55th Conference on*. IEEE, 2016, pp. 3381–3388.

[9] K. Dantu, B. Kate, J. Waterman, P. Bailis, and M. Welsh, "Programming micro-aerial vehicle swarms with karma," in *Proceedings of the 9th ACM Conference on Embedded Networked Sensor Systems*. ACM, 2011, pp. 121–134.

[10] M. V. Srinivasan, R. J. Moore, S. Thurrowgood, D. Soccol, and D. Bland, "From biology to engineering: insect vision and applications to robotics," in *Frontiers in sensing*. Springer, 2012, pp. 19–39.

[11] R. C. Leishman, J. C. Macdonald, R. W. Beard, and T. W. McLain, "Quadrotors and accelerometers: State estimation with an improved dynamic model," *IEEE Control Systems*, vol. 34, no. 1, pp. 28–41, 2014.

[12] T. Madani and A. Benallegue, "Backstepping control for a quadrotor helicopter," in *Intelligent Robots and Systems, 2006 IEEE/RSJ International Conference on*. IEEE, 2006, pp. 3255–3260.

[13] ——, "Control of a quadrotor mini-helicopter via full state backstepping technique," in *Decision and Control, 2006 45th IEEE Conference on*. IEEE, 2006, pp. 1515–1520.

[14] R. Xu and U. Ozguner, "Sliding mode control of a quadrotor helicopter," in *Decision and Control, 2006 45th IEEE Conference on*. IEEE, 2006, pp. 4957–4962.

[15] S. Bouabdallah, "Design and control of quadrotors with application to autonomous flying," Ph.D. dissertation, Ecole Polytechnique Federale de Lausanne, 2007.

[16] T. Bresciani, "Modelling, identification and control of a quadrotor helicopter," *MSc Theses*, 2008.

[17] C. Luis and J. L. Ny, "Design of a trajectory tracking controller for a nanoquadcopter," *arXiv preprint arXiv:1608.05786*, 2016.

[18] G. P. Subramanian, "Nonlinear control strategies for quadrotors and cubesats," Ph.D. dissertation, University of Illinois at Urbana-Champaign, 2015.